

Article

Cationically Modified Nanocrystalline Cellulose/Carboxyl-Functionalized Graphene Quantum Dots Nanocomposite Thin Film: Characterization and Potential Sensing Application

Najwa Norimanina Muhammad Rosddi ¹, Yap Wing Fen ^{1,2,*} , Nur Ain Asyiqin Anas ^{2,3},
Nur Alia Sheh Omar ², Nur Syahira Md Ramdzan ¹ and
Wan Mohd Ebtisyam Mustaqim Mohd Daniyal ²

¹ Department of Physics, Faculty of Science, Universiti Putra Malaysia, UPM Serdang 43400, Selangor, Malaysia; najwanorimanina@gmail.com (N.N.M.R.); nursyahira.upm@gmail.com (N.S.M.R.)

² Functional Devices Laboratory, Institute of Advanced Technology, Universiti Putra Malaysia, UPM Serdang 43400, Selangor, Malaysia; nurainanas.upm@gmail.com (N.A.A.A.); nuralia.upm@gmail.com (N.A.S.O.); wanmdsyam@gmail.com (W.M.E.M.M.D.)

³ Physics Unit, Centre of Foundation Studies for Agricultural Science, Universiti Putra Malaysia, UPM Serdang 43400, Selangor, Malaysia

* Correspondence: yapwingfen@gmail.com; Tel.: +60-39769-6689

Received: 5 August 2020; Accepted: 5 September 2020; Published: 27 September 2020



Abstract: In this study, highly functional cationically modified nanocrystalline cellulose (NCC)/carboxyl-functionalized graphene quantum dots (CGQD) has been described. The surface of NCC was first modified with hexadecyltrimethylammonium bromide (CTA) before combining with CGQD. The CGQD, CTA-NCC and CTA-NCC/CGQD nanocomposites thin films were prepared using spin coating technique. The obtained nanocomposite thin films were then characterized by using the Fourier transform infrared spectroscopy (FTIR) which confirmed the existence of hydroxyl groups, carboxyl groups and alkyl groups in CTA-NCC/CGQD. The optical properties of the thin films were characterized using UV–Vis spectroscopy. The absorption of CTA-NCC/CGQD was high with an optical band gap of 4.127 eV. On the other hand, the CTA-NCC/CGQD nanocomposite thin film showed positive responses towards glucose solution of different concentration using an optical method based on surface plasmon resonance phenomenon. This work suggests that the novel nanocomposite thin film has potential for a sensing application in glucose detection.

Keywords: nanocrystalline cellulose; graphene quantum dots; thin film; optical; sensing; glucose; surface plasmon resonance

1. Introduction

In recent years, there has been an interest in the production of nanocrystalline cellulose (NCC) from cellulosic material because of its biodegradability, renewability, abundance and excellent mechanical properties [1]. In this world, cellulose is one of the most numerous natural renewable and biodegradable polysaccharides. NCC is the nano-scaled of needle or rod-shaped crystalline which has hundreds of nanometers in length and 1–10 nm in width [2,3]. NCC is obtained when cellulose undergoes acid hydrolysis with conditions where the amorphous regions are selectively hydrolyzed [4]. Mineral acids including hydrochloric acid and sulfuric acid are used in the mixture of hydrolysis of cellulose to prepare NCC [5]. Thus, NCC is constitutively acidic and exhibits a lyotropic phase behavior

depending on the concentration. NCC has the potential in various applications as a rheology modifier such as drilling fluids, consumer products, drug delivery, artificial tissue formation and injectable hydrogels [6–8].

To enhance the NCC properties, the hydroxyl functional group in NCC can be modified by using several methods [9–12]. In this present work, NCC has been cationically modified using hexadecyltrimethylammonium bromide (CTA). CTA can enhance the absorption by improving hyperchromicity and sensitization of NCC [13–17]. To further increase the performance, this modified NCC was chosen as a matrix for carboxyl functionalized graphene quantum dots (CGQD) as CGQD has beneficial and unique properties including hydrophilicity, strong photoluminescence and photo-stability [18–20]. Due to its outstanding properties, CGQD provides unprecedented opportunities for different fields of application such as optical sensing, catalysis and bioimaging [21–25].

As far as we know, the optical properties of the CTA cationically modified NCC/CGQD (CTA-NCC/CGQD) nanocomposite thin film and its potential application for detection of glucose using surface plasmon resonance technique (SPR) have yet to be reported. SPR is known as a simple optical method for surface studies of thin films and can act as a very sensitive spectroscopy for detection of a variety of targets [26–42]. Hence in this study, the fabrication of the CTA-NCC/CGQD nanocomposite thin film, its characterization and potential sensing application were explored.

2. Materials and Methods

2.1. Reagent and Materials

Hexadecyltrimethyl ammonium bromide (CTA) and nanocrystalline cellulose (NCC) were purchased from Sigma Aldrich (St. Louis, MO, USA). Carboxyl-graphene quantum dots (CGQD) solution (0.1 wt%) was purchased from ACS Material (Pasadena, CA, USA) and glucose was purchased from R&M Marketing (Essex, UK).

2.2. Preparation of Chemicals

To prepare NCC solution, 1 g of NCC was diluted in 100 mL deionized water. Then, 0.2 g of CTA was diluted in 20 mL of deionized water to obtain CTA solution. NCC solution was then dropped into CTA solution drop by drop while heat stirred for 24 h. The CTA-NCC solution was centrifuged at 3000 rpm for 15 min. Then, CTA-NCC/CGQD solution (0.05 wt%) was obtained by dispersing 1 mL of CGQD into 1 mL of CTA-NCC. The glucose solution was prepared by dissolving 9.91 mg of glucose with 100 mL of deionized water to produce 10 μ M of glucose solution. To prepare glucose solution with various concentration, the 10 μ M of glucose solution was diluted with deionized water based on the formula $M_1V_1 = M_2V_2$ to obtain 0.005, 0.01, 0.03, 0.05 and 0.1 μ M of glucose [43–45].

2.3. Preparation of CTA-NCC/CGQD Nanocomposite Thin Film

Glass cover slips (24 mm \times 24 mm \times 0.1 mm) were used as the substrates. The glass slip was first sputtered with gold (SC7640 sputter coater machine) for 67 seconds to obtain 50 nm of gold thin film [46–48]. Then, spin coating technique was used to deposit the CTA-NCC/CGQD solution homogeneously on the gold surface. About 1000 μ L of CTA-NCC/CGQD solution was added on a gold coated glass slip and was spun at 3000 rev/min for 30 seconds using spin coater P-6708D to obtain around 12–15 nm thickness of the CTA-NCC/CGQD layer. The summarized flow chart for the preparation of CTA-NCC/CGQD is shown in Figure 1.



Figure 1. Preparation of hexadecyltrimethylammonium bromide (CTA)-nanocrystalline cellulose (NCC)/carboxyl-functionalized graphene quantum dots (CGQD) thin film.

2.4. Characterization Instrument

The Fourier transform infrared (FTIR) spectrum of CGQD, CTA-NCC and CTA-NCC/CGQD solutions were analyzed using the Fourier Transform Infrared Spectrometer model spectrum 100 (PerkinElmer, Waltham, MA, USA), with wavelength set from 400 to 4000 cm^{-1} which is to determine the functional groups and the chemical interaction of the composites. Other than that, the purity of the compound can be obtained from the collection of the absorption band from the spectrum. For optical properties, the absorption of all samples with wavelength range from 220 nm to 500 nm was investigated using UV-Vis-NIR spectrometer (UV-3600 Shimadzu, Kyoto, Japan). The absorbance coated thin film was measured at room temperature. The energy band gap was determined by analyzing the graph of absorption peak against wavelength obtained using UV-Vis spectrometer.

2.5. Surface Plasmon Resonance

Surface plasmon resonance (SPR) is used to identify the potential of CTA-NCC/CGQD nanocomposite thin film for glucose detection. SPR is an optical process in which light satisfying resonance conditions excite a charge-density wave propagating along the interface between a dielectric material and metal by p-polarized and monochromatic light beam [49]. The reflected light intensity is reduced at a specific incident angle producing a sharp shadow due to the resonance occurs between surface plasmon wave and incident beam [50]. The SPR measurement was carried out by determining the reflected He-Ne laser beam (532.8 nm, 5 mW) [51]. Figure 2 shows the setup of SPR sensor. The SPR setup consisted of an He-Ne laser, a light attenuator, a polarizer and optical chopper (SR 540) and an optical stage driven by a stepper motor MM 3000 with a resolution of 0.001° (Newport, CA, USA). The reflected beam was detected by photodiode and then processed by the lock-in-amplifier (SR530) [52–55].

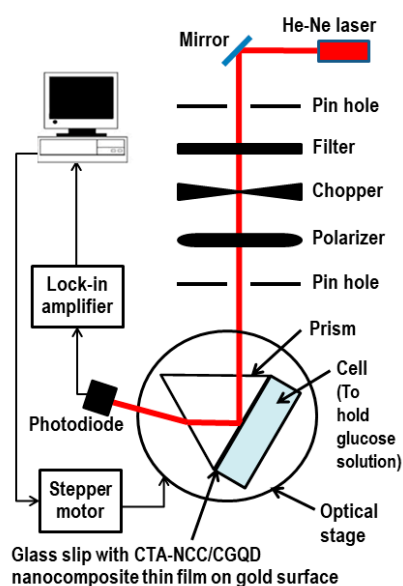


Figure 2. Experimental setup of surface plasmon resonance (SPR) sensor.

3. Results

3.1. FTIR Analysis

The FTIR spectrum of CGQD, CTA-NCC and CTA-NCC/CGQD solutions are shown in Figure 3. From the spectrum of the CGQD solution, the peak present at 3310 cm^{-1} represented O–H stretching. The peak at 2891 cm^{-1} was attributed to the C–H stretching. The characteristic band appearing at 1625 cm^{-1} corresponded to the stretching of C=O of the carboxylic group in graphene quantum dots and the peak at 1037 cm^{-1} represented the C–O stretching [18].

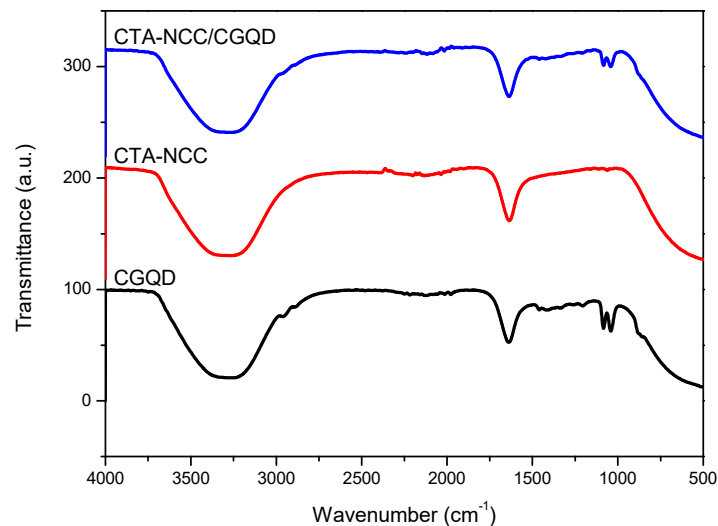


Figure 3. FTIR spectrum of CGQD, CTA-NCC and CTA-NCC/CGQD solutions.

Next, in the spectrum of CTA-NCC solution, the peak at 3332 cm^{-1} corresponded to the O–H stretching. The peak at 1617 cm^{-1} was attributed to the stretching vibration of C–O and the peak at 1056 cm^{-1} corresponded to C–O stretching [56].

The spectra of CTA-NCC/CGQD solution displayed the properties similar to CGQD and CTA-NCC thin film where there was a broad absorption peak at 3277 cm^{-1} that was attributed to the O–H stretching vibration. The peak at 2885 cm^{-1} corresponded to C–H stretching. The peak at 1637 cm^{-1} can be assigned to C=O stretching and is similar to the peak for both spectrums of CGQD and CTA-NCC. The characteristics band that appeared at 1032 cm^{-1} corresponded to the stretching of C–O. From the results, it is successfully confirmed that the functional groups of O–H, C–H, C=O and C–O existed in the composite solution. CGQD that are rich with oxygen-containing groups might interact with the hydroxyl groups and oxygen atoms in CTA-NCC through the hydrogen bonding. Furthermore, the possible structure of the composite is also presented in Figure 4.

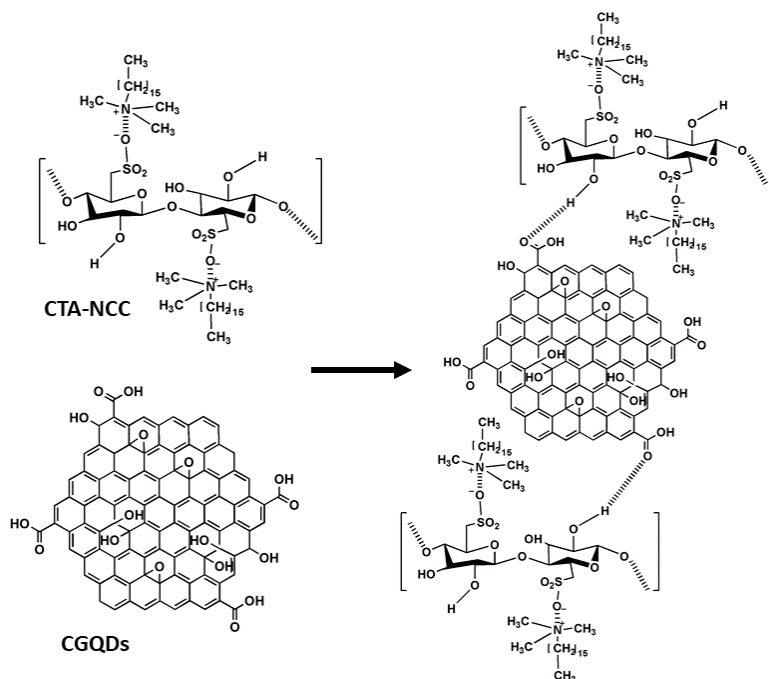


Figure 4. The possible structure of CTA-NCC/CGQD nanocomposite.

3.2. Optical Studies

The optical properties were analyzed using the absorbance spectrum of the thin film with wavelength range 220–500 nm. The absorbance curves for CGQD, CTA-NCC and CTA-NCC/CGQD thin film are presented in Figure 5.

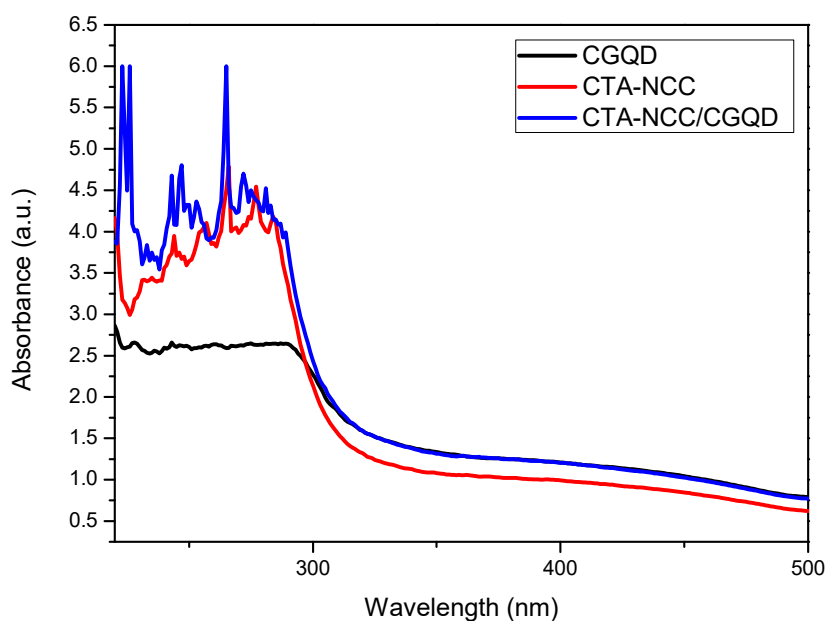


Figure 5. Absorbance spectrum of CGQD, CTA-NCC and CTA-NCC/CGQD thin film.

As shown in Figure 5, the absorbance curve for the thin film is different. From the figure, the CTA-NCC/CGQD thin film shows the highest absorption spectra with the absorption peaks at 222.9 nm, 225.9 nm and 264.9 nm. The highest absorption was contributed by the modification of CGQD with CTA-NCC, which confirmed the presence plasmon resonance in carbonaceous material [57]. On the other hand, the lowest absorbance belongs to CGQD thin film. The characteristic peaks that

appeared in the nanocomposite thin film can be attributed to the presence of $\pi \rightarrow \pi^*$ bond transitions of the carbonyl groups [58]. In addition, it can be observed that the maximum absorption length can be determined from 263.04 nm to 266.63 nm. The results obtained are in the range of the absorption peaks for sulfur doped graphene quantum dots which are at 216–464 nm [59].

To proceed with the determination of the optical band gap, the relationship between the absorbance and the intensities of the monochromatic light was used [60]. The absorbance, A of samples can be related with the ratio of the initial light intensity on the detector I_0 to the light intensity with the presence of the sample I_t .

$$A = \log_{10} \frac{I_0}{I_t} \quad (1)$$

The absorbance coefficient is another quantity that can be measured. It is a very useful quantity which is used to compare samples of a varying thickness. The absorbance coefficient, α can be expressed as

$$\alpha = 2.303 \frac{A}{t} \quad (2)$$

where t is the thin film thickness in meters and the α is in units of m^{-1} . The energy band gap of these composites has been figured out with the help of the absorption coefficient. To obtain the optical band gap from the absorption spectra, the Tauc relation is used:

$$\alpha = \frac{k(h\nu - E_g)^n}{h\nu} \quad (3)$$

where k is a constant, h is the Plank's constant, ν is the frequency of the incident photon, the multiplication of h and ν , $h\nu$ represents the incident photon energy, E_g is the optical band gap and n is the state of transition. In this study we use $n = 1/2$ for direct transitions. Rearranging Equation (3) gives

$$(\alpha h\nu)^2 = k(h\nu - E_g) \quad (4)$$

Based on Equation (4), a graph of $(\alpha h\nu)^2$ against $h\nu$ can be plotted using linear fitting techniques and the optical band gap of the thin films can be determined [61–63]. According to Abdulla and Abbo (2012), the intersection of the straight line on the x-axis is taken as the value of the optical band gap [64]. The graph of $(\alpha h\nu)^2$ versus $h\nu$ for CGQD thin film, CTA-NCC thin film and CTA-NCC/CGQD thin film are shown in Figures 6–8, respectively.

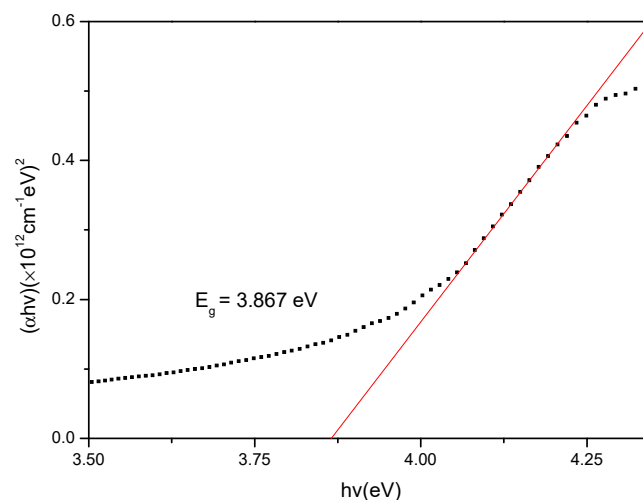


Figure 6. Optical band gap for CGQD thin film.

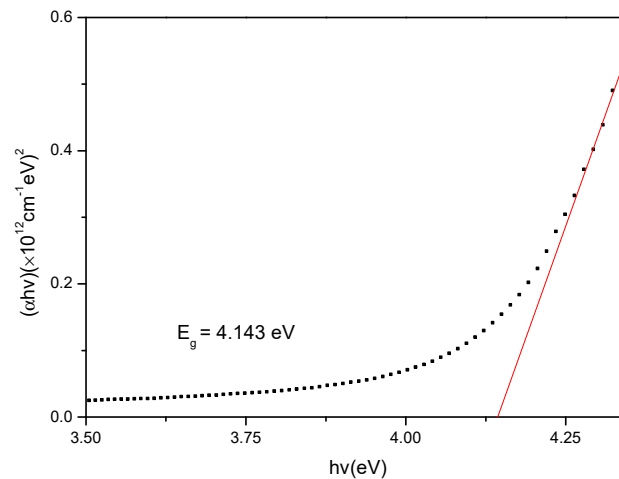


Figure 7. Optical band gap for CTA-NCC thin film.

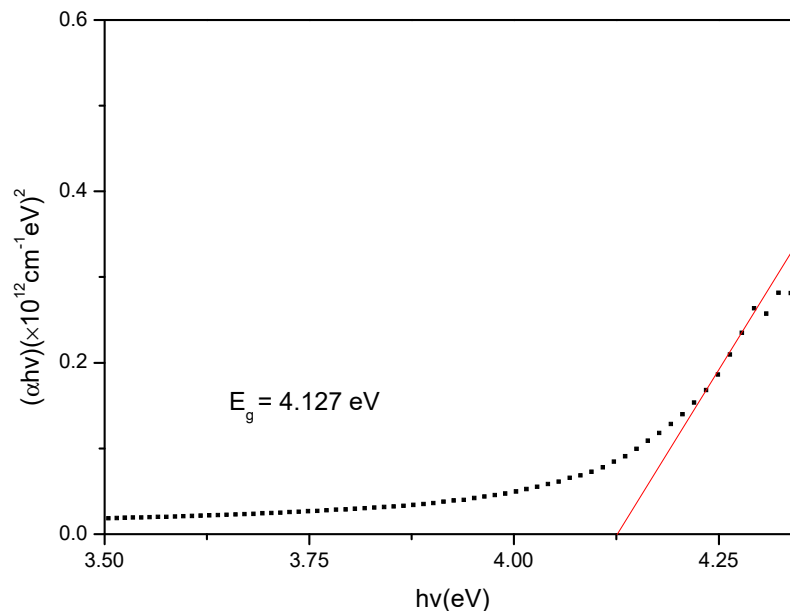


Figure 8. Optical band gap for CTA-NCC/CGQD thin film.

As can be seen from the figures, the intersection of the linear fitted line on the x-axis gives the value of the optical band gap. The term band gap is denoting the energy difference between the top of the valence band to the bottom of the conduction band where electrons can jump from one band to another. It necessitates a specific minimum extent of energy for the transition to permit an electron to jump from a valence band to a conduction band and this energy is called as the band gap energy. The optical band gap energies of CGQD, CTA-NCC and CTA-NCC/CGQD are 3.867 eV, 4.143 eV and 4.127 eV, respectively. Based on the result, CTA-NCC had the highest band gap energy among energy band gap results of all three thin films. The variations of optical band gap for the composite thin films, probably due to the presence of CTA-NCC solution as the band gap of CTA-NCC/CGQD, is higher than CGQD. The CTA-NCC/CGQD has a higher energy band gap as compared to CGQD thin film, which is in good agreement with the work reported by Daniyal et al. (2018), i.e., CTA-NCC increased the optical band gap of the composite [56].

3.3. Potential Sensing Analysis

The SPR experiment was first conducted using gold CTA-NCC/CGQD nanocomposite thin film in contact with deionized water (or 0 μM of glucose). The resonance angle for the first part

of this experiment was obtained as 54.400° , where this value was used to compare the resonance angle for different concentrations of glucose solution. The SPR experiment was then continued for different concentrations of glucose solution that ranged from $0.005 \mu\text{M}$ to $0.1 \mu\text{M}$. The glucose solution was injected into the cell one after another [65]. The reflectance as a function of incident angle of CTA-NCC/CGQD thin film, in contact with different concentrations of glucose solutions is shown in Figure 7. From the curves, the resonance angle can be obtained for the glucose concentration of 0.005 , 0.01 , 0.03 , 0.05 and $0.1 \mu\text{M}$.

From Figure 9, it can be observed that the resonance angle was shifted to the right and it further increased with the increase of glucose concentration [66,67]. The resonance angles obtained for 0.005 , 0.01 , 0.03 , 0.05 and $0.1 \mu\text{M}$ were 54.571° , 54.732° , 54.755° , 54.767° and 54.769° , respectively. The shift of the SPR curves and resonance angle change demonstrated that the CTA-NCC/CGQD nanocomposite thin film has affinity towards glucose, where its incorporation with SPR can be a potential sensor for glucose.

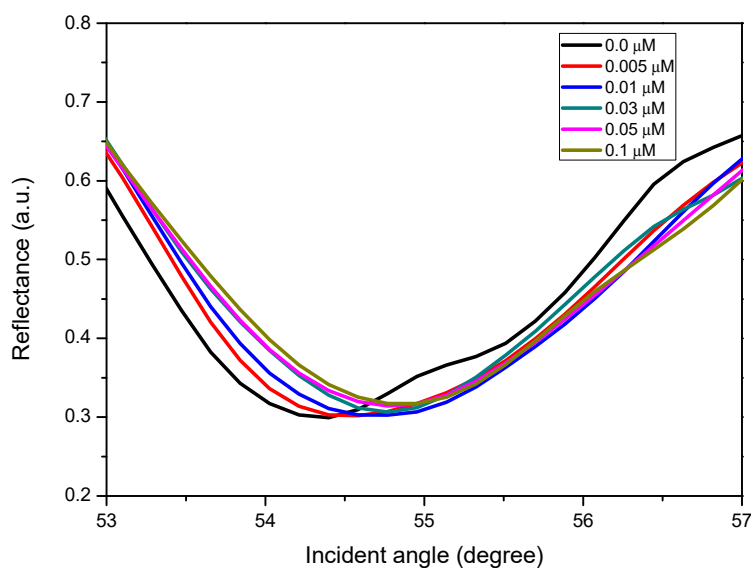


Figure 9. SPR curves for CTA-NCC/CGQD nanocomposite thin film for glucose solution with different concentrations (0.0 – $0.1 \mu\text{M}$).

4. Conclusions

In this study, the CTA cationically modified NCC/CGQD nanocomposite thin film has been successfully fabricated. The functional groups that existed in the thin film were confirmed from the FTIR results. The absorbance value of CTA-NCC/CGQD was the highest with energy band gap of 4.127 eV . The studies of the CTA-NCC/CGQD nanocomposite thin film using the SPR technique have successfully shown that the novel thin film can detect various concentrations of glucose with the lowest detection of 5 nM . This study gives an important idea that the CTA-NCC/CGQD nanocomposite thin film has high potential as an application in sensing glucose when incorporated with the SPR technique and can be further investigated in future studies.

Author Contributions: Conceptualization, methodology, writing—original draft preparation, N.N.M.R.; validation, supervision, writing—review and editing, funding acquisition, Y.W.F.; investigation, formal analysis, N.A.A.A.; software, resources, N.A.S.O.; visualization, N.S.M.R. and W.M.E.M.M.D. All authors have read and agreed to the published version of the manuscript.

Funding: This research was funded and supported by the Ministry of Education Malaysia through the Fundamental Research Grant Scheme (FRGS) (FRGS/1/2019/STG02/UPM/02/1) and Putra Grant Universiti Putra Malaysia.

Acknowledgments: The authors acknowledged the laboratory facilities provided by the Institute of Advanced Technology, Department of Physics, and Department of Chemistry, Universiti Putra Malaysia.

Conflicts of Interest: The authors declare no conflict of interest.

References

1. Azrinaa, Z.A.Z.; Beg, M.D.H.; Rosli, M.Y.; Ramli, R.; Junadi, N.; Alam, A.K.M.M. Spherical nanocrystalline cellulose (NCC) from oil palm empty fruitbunch pulp via ultrasound assisted hydrolysis. *Carbohydr. Polym.* **2017**, *162*, 115–120. [[CrossRef](#)] [[PubMed](#)]
2. Daniyal, W.M.E.M.M.; Fen, Y.W.; Abdullah, J.; Sadrolhosseini, A.R.; Saleviter, S.; Omar, N.A.S. Exploration of surface plasmon resonance for sensing copper ion based on nanocrystalline cellulose-modified thin film. *Opt. Express* **2018**, *26*, 34880–34893. [[CrossRef](#)] [[PubMed](#)]
3. Junior, E.A.P.; Dávila, J.L.; d'Ávila, M.A. Rheological studies on nanocrystalline cellulose/alginate suspensions. *J. Mol. Liq.* **2019**, *277*, 418–423.
4. Kaboorani, A.; Riedl, B.; Blanchet, P.; Fellin, M.; Hosseinaei, O.; Wang, S. Nanocrystalline cellulose (NCC): A renewable nanomaterial for polyvinyl acetate (PVA) adhesive. *Eur. Polym. J.* **2012**, *48*, 1829–1837. [[CrossRef](#)]
5. Sun, Y.; Liu, P.; Liu, Z. Catalytic conversion of carbohydrates to 5-hydroxymethylfurfural from the waste liquid of acid hydrolysis NCC. *Carbohydr. Polym.* **2016**, *142*, 177–182. [[CrossRef](#)] [[PubMed](#)]
6. Li, M.C.; Wu, Q.; Song, K.; Qing, Y.; Wu, Y. Cellulose nanoparticles as modifiers for rheology and fluid loss in bentonite water-based fluids. *ACS Appl. Mater. Interfaces* **2015**, *7*, 5006–5016. [[CrossRef](#)]
7. Taheri, A.; Mohammadi, M. The use of cellulose nanocrystals for potential application in topical delivery of hydroquinone. *Chem. Biol. Drug Des.* **2015**, *86*, 102–106. [[CrossRef](#)]
8. Yang, Y.; Chen, Z.; Zhang, J.; Wang, G.; Zhang, R.; Suo, D. Preparation and Applications of the Cellulose Nanocrystal. *Int. J. Polym. Sci.* **2019**, *2019*, 1767028. [[CrossRef](#)]
9. Daniyal, W.M.E.M.M.; Fen, Y.W.; Anas, N.A.A.; Omar, N.A.S.; Ramdzan, N.S.M.; Nakajima, H.; Mahdi, M.A. Enhancing the sensitivity of a surface plasmon resonance-based optical sensor for zinc ion detection by the modification of a gold thin film. *RSC Adv.* **2019**, *9*, 41729–41736. [[CrossRef](#)]
10. Salajková, M.; Berglund, L.A.; Zhou, Q. Hydrophobic cellulose nanocrystals modified with quaternary ammonium salts. *J. Mater. Chem.* **2012**, *22*, 19798–19805. [[CrossRef](#)]
11. Grunert, M.; Winter, W.T. Nanocomposites of cellulose acetate butyrate reinforced with cellulose nanocrystals. *J. Polym. Environ.* **2002**, *10*, 27–30. [[CrossRef](#)]
12. Abitbol, T.; Marway, H.; Cranston, E.D. Surface modification of cellulose nanocrystals with cetyltrimethylammonium bromide. *Nord. Pulp Pap. Res. J.* **2014**, *29*, 7764–7779. [[CrossRef](#)]
13. Mao, Y.; Fan, Q.; Li, J.; Yu, L.; Qu, L.-B. A novel and green CTAB-functionalized graphene nanosheets electrochemical sensor for Sudan I determination. *Sens. Actuators B Chem.* **2014**, *203*, 759–765. [[CrossRef](#)]
14. Selvi, S.S.T.; Linet, J.M.; Sagadevan, S. Influence of CTAB surfactant on structural and optical properties of CuS and CdS nanoparticles by hydrothermal route. *J. Exp. Nanosci.* **2018**, *13*, 130–143. [[CrossRef](#)]
15. Yao, P.J.; Wang, J.; Du, H.Y.; Zhao, L.; Yan, W.P. Effect of CTAB concentration on synthesis and sensing properties of perovskite oxide via a hydrothermal process. *Key Eng. Mater.* **2013**, *543*, 330–333. [[CrossRef](#)]
16. Jin, Y.; Liu, F.; Tong, M.; Hou, Y. Removal of arsenate by cetyltrimethylammonium bromide modified magnetic nanoparticles. *J. Hazard. Mater.* **2012**, *227*, 461–468. [[CrossRef](#)]
17. Leng, Y.; Qian, S.; Wang, Y.; Lu, C.; Ji, X.; Lu, Z.; Lin, H. Single-indicator-based multidimensional sensing: Detection and identification of heavy metal ions and understanding the foundations from experiment to simulation. *Sci. Rep.* **2016**, *6*, 25354. [[CrossRef](#)]
18. Ramdzan, N.S.M.; Fen, Y.W.; Omar, N.A.S.; Saleviter, S.; Zainudin, A.A. Optical and surface plasmon resonance sensing properties for chitosan/carboxyl-functionalized graphene quantum dots thin film. *Optik* **2019**, *178*, 802–812. [[CrossRef](#)]
19. Shen, S.; Wang, J.; Wu, Z.; Du, Z.; Tang, Z.; Wu, X. Graphene quantum dots with high yield and high quality synthesized from low cost precursor of aphanitic graphite. *Nanomaterials* **2020**, *10*, 375. [[CrossRef](#)]
20. Kaciulis, S.; Mezzi, A.; Soltani, P.; Pizzoferrato, R.; Ciotta, E.; Proposito, P. Graphene quantum dots obtained by unfolding fullerene. *Thin Solid Films* **2019**, *673*, 19–25. [[CrossRef](#)]
21. Li, L.; Li, L.; Wang, C.; Liu, K.; Zhu, R.; Qiang, H.; Lin, Y. Synthesis of nitrogen-doped and amino acid-functionalized graphene quantum dots from glycine, and their application to the fluorometric determination of ferric ion. *Microchim. Acta* **2014**, *182*, 763–770. [[CrossRef](#)]

22. Tang, Y.; Li, J.; Guo, Q.; Nie, G. An ultrasensitive electrochemiluminescence assay for Hg²⁺ through graphene quantum dots and poly(5-formylindole) nanocomposite. *Sens. Actuators B Chem.* **2019**, *282*, 824–830. [[CrossRef](#)]
23. Tian, P.; Tang, L.; Teng, K.S.; Lau, S.P. Graphene quantum dots from chemistry to applications. *Mater. Today Chem.* **2018**, *10*, 221–258. [[CrossRef](#)]
24. Li, Y.; Hu, Y.; Zhao, Y.; Shi, G.; Deng, L.; Hou, Y.; Qu, L. An electrochemical avenue to green-luminescent graphene quantum dots as potential electron-acceptors for photovoltaics. *Adv. Mater.* **2010**, *23*, 776–780. [[CrossRef](#)] [[PubMed](#)]
25. Kováčová, M.; Špitalská, E.; Markovic, Z.; Špitálský, Z. Carbon quantum dots as antibacterial photosensitizers and their polymer nanocomposite applications. *Part. Part. Syst. Charact.* **2020**, *37*, 1900348. [[CrossRef](#)]
26. Fen, Y.W.; Yunus, W.M.M. Surface plasmon resonance spectroscopy as an alternative for sensing heavy metal ions: A review. *Sens. Rev.* **2013**, *33*, 305–314.
27. Omar, N.A.S.; Fen, Y.W.; Saleviter, S.; Daniyal, W.M.E.M.M.; Anas, N.A.A.; Ramdzan, N.S.M.; Roshidi, M.D.A. Development of a graphene-based surface plasmon resonance optical sensor chip for potential biomedical application. *Materials* **2019**, *12*, 1928. [[CrossRef](#)]
28. Anas, N.A.A.; Fen, Y.W.; Omar, N.A.S.; Daniyal, W.M.E.M.M.; Ramdzan, N.S.M.; Saleviter, S. Development of graphene quantum dots-based optical sensor for toxic metal ion detection. *Sensors* **2019**, *19*, 3850. [[CrossRef](#)]
29. Eddin, F.B.K.; Fen, Y.W. The principle of nanomaterials based surface plasmon resonance biosensors and its potential for dopamine detection. *Molecules* **2020**, *25*, 2769. [[CrossRef](#)] [[PubMed](#)]
30. Hashim, H.S.; Fen, Y.W.; Omar, N.A.S.; Omar, N.A.S.; Abdullah, J.; Daniyal, W.M.E.M.M.; Saleviter, S. Detection of phenol by incorporation of gold modified-enzyme based graphene oxide thin film with surface plasmon resonance technique. *Opt. Express* **2020**, *28*, 9738–9752. [[CrossRef](#)] [[PubMed](#)]
31. Daniyal, W.M.E.M.M.; Saleviter, S.; Fen, Y.W. Development of surface plasmon resonance spectroscopy for metal ion detection. *Sens. Mater.* **2018**, *30*, 2023–2038. [[CrossRef](#)]
32. Jia, Y.; Peng, Y.; Bai, J.; Zhang, X.; Cui, Y.; Ning, B.; Cui, J.; Gao, Z. Magnetic nanoparticle enhanced surface plasmon resonance sensor for estradiol analysis. *Sens. Actuators B Chem.* **2017**, *254*, 629–635. [[CrossRef](#)]
33. Fen, Y.W.; Yunus, W.M.M.; Yusof, N.A. Surface plasmon resonance optical sensor for detection of essential heavy metal ions with potential for toxicity: Copper, zinc and manganese ions. *Sens. Lett.* **2011**, *9*, 1704–1711. [[CrossRef](#)]
34. Fen, Y.W.; Yunus, W.M.M.; Yusof, N.A. Detection of mercury and copper ions using surface plasmon resonance optical sensor. *Sens. Mater.* **2011**, *23*, 325–334.
35. Zainudin, A.A.; Fen, Y.W.; Yusof, N.A.; Al-Rekabi, S.H.; Mahdi, M.A.; Omar, N.A.S. Incorporation of surface plasmon resonance with novel valinomycin doped chitosan-graphene oxide thin film for sensing potassium ion. *Spectrochim. Acta A Mol. Biomol. Spectrosc.* **2018**, *191*, 111–115. [[CrossRef](#)]
36. Omar, N.A.S.; Fen, Y.W. Recent development of SPR spectroscopy as potential method for diagnosis of dengue virus E-protein. *Sens. Rev.* **2018**, *38*, 106–116. [[CrossRef](#)]
37. Saleviter, S.; Fen, Y.W.; Omar, N.A.S.; Zainudin, A.A.; Yusof, N.A. Development of optical sensor for determination of Co(II) based on surface plasmon resonance phenomenon. *Sens. Lett.* **2017**, *15*, 862–867. [[CrossRef](#)]
38. Fen, Y.W.; Yunus, W.M.M.; Talib, Z.A. Analysis of Pb(II) ion sensing by crosslinked chitosan thin film using surface plasmon resonance spectroscopy. *Optik* **2013**, *124*, 126–133. [[CrossRef](#)]
39. Ramdzan, N.S.M.; Fen, Y.W.; Anas, N.A.A.; Omar, N.A.S.; Saleviter, S. Development of biopolymer and conducting polymer-based optical sensors for heavy metal ion detection. *Molecules* **2020**, *25*, 2548. [[CrossRef](#)]
40. Anas, N.A.A.; Fen, Y.W.; Omar, N.A.S.; Ramdzan, N.S.M.; Daniyal, W.M.E.M.M.; Saleviter, S.; Zainudin, A.A. Optical properties of chitosan/hydroxyl-functionalized graphene quantum dots thin film for potential optical detection of ferric(III) ion. *Opt. Laser Technol.* **2019**, *120*, 105724. [[CrossRef](#)]
41. Al-Rekabi, S.H.; Kamil, Y.M.; Bakar, M.H.A.; Fen, Y.W.; Lim, H.N.; Kanagesan, S.; Mahdi, M.A. Hydrous ferric oxide-magnetite-reduced graphene oxide nanocomposite for optical detection of arsenic using surface plasmon resonance. *Opt. Laser Technol.* **2019**, *111*, 417–423. [[CrossRef](#)]
42. Fen, Y.W.; Yunus, W.M.M.; Talib, Z.A.; Yusof, N.A. Development of surface plasmon resonance sensor for determining zinc ion using novel active nanolayers as probe. *Spectrochim. Acta A Mol. Biomol. Spectrosc.* **2015**, *134*, 48–52. [[CrossRef](#)]

43. Saleviter, S.; Fen, Y.W.; Daniyal, W.M.E.M.M.; Abdullah, J.; Sadrolhosseini, A.R.; Omar, N.A.S. Design and analysis of surface plasmon resonance optical sensor for determining cobalt ion based on chitosan-graphene oxide decorated quantum dots-modified gold active layer. *Opt. Express* **2019**, *27*, 32294–32307. [[CrossRef](#)] [[PubMed](#)]
44. Omar, N.A.S.; Fen, Y.W.; Abdullah, J.; Sadrolhosseini, A.R.; Kamil, Y.M.; Fauzi, N.I.F.; Hashim, H.S.; Mahdi, M.A. Quantitative and selective surface plasmon resonance response based on a reduced graphene oxide-polyamidoamine nanocomposite for detection of dengue virus e-proteins. *Nanomaterials* **2020**, *10*, 569. [[CrossRef](#)] [[PubMed](#)]
45. Fen, Y.W.; Yunus, W.M.M.; Yusof, N.A. Optical properties of crosslinked chitosan thin film as copper ion detection using surface plasmon resonance technique. *Opt. Appl.* **2011**, *41*, 999–1013.
46. Roshidi, D.A.; Fen, Y.W.; Daniyal, W.M.E.M.M.; Omar, N.A.S.; Zulholinda, M. Structural and optical properties of chitosan-poly(amidoamine) dendrimer composite thin film for potential sensing Pb²⁺ using an optical spectroscopy. *Optik* **2019**, *185*, 351–358. [[CrossRef](#)]
47. Omar, N.A.S.; Fen, Y.W.; Abdullah, J.; Zaid, M.H.M.; Daniyal, W.M.E.M.M.; Mahdi, M.A. Sensitive surface plasmon resonance performance of cadmium sulfide quantum dots-amine functionalized graphene oxide based thin film towards dengue virus E-protein. *Opt. Laser Technol.* **2019**, *114*, 204–208. [[CrossRef](#)]
48. Anas, N.A.A.; Fen, Y.W.; Yusof, N.A.; Omar, N.A.S.; Ramdzan, N.S.M.; Daniyal, W.M.E.M.M. Investigating the properties of cetyltrimethylammonium bromide/hydroxylated graphene quantum dots thin film for potential optical detection of heavy metal ions. *Materials* **2020**, *13*, 2591. [[CrossRef](#)]
49. Homola, J. Surface plasmon resonance sensors for detection of chemical and biological species. *Chem. Rev.* **2008**, *108*, 462–493. [[CrossRef](#)]
50. Fen, Y.W.; Yunus, W.M.M. Utilization of chitosan-based sensor thin films for the detection of lead ion by surface plasmon resonance optical sensor. *IEEE Sens. J.* **2013**, *13*, 1413–1418. [[CrossRef](#)]
51. Fen, Y.W.; Yunus, W.M.M.; Yusof, N.A. Surface plasmon resonance optical sensor for detection of Pb²⁺ based on immobilized p-tert-butylcalix[4]arene-tetrakis in chitosan thin film as an active layer. *Sens. Actuators B Chem.* **2012**, *171–172*, 287–293. [[CrossRef](#)]
52. Saleviter, S.; Fen, Y.W.; Omar, N.A.S.; Daniyal, W.M.E.M.M.; Abdullah, J.; Zaid, M.H.M. Structural and optical studies of cadmium sulfide quantum dot-graphene oxide-chitosan nanocomposite thin film as a novel SPR spectroscopy active layer. *J. Nanomater.* **2018**, *2018*, 4324072. [[CrossRef](#)]
53. Zainudin, A.A.; Fen, Y.W.; Yusof, N.A.; Omar, N.A.S. Structural, optical and sensing properties of ionophore doped graphene based bionanocomposite thin film. *Optik* **2017**, *144*, 308–315. [[CrossRef](#)]
54. Fen, Y.W.; Yunus, W.M.M.; Moxsin, M.M.; Talib, Z.A.; Yusof, N.A. Surface plasmon resonance optical sensor for mercury ion detection by crosslinked chitosan thin film. *J. Optoelectron. Adv. Mater.* **2011**, *13*, 279–285.
55. Fauzi, N.I.M.; Fen, Y.W.; Omar, N.A.S.; Saleviter, S.; Daniyal, W.M.E.M.M.; Hashim, H.S.; Nasrullah, M. Nanostructured chitosan/maghemite composites thin film for potential optical detection of mercury ion by surface plasmon resonance investigation. *Polymers* **2020**, *12*, 1497. [[CrossRef](#)]
56. Daniyal, W.M.E.M.M.; Fen, Y.W.; Abdullah, J.; Saleviter, S.; Omar, N.A.S. Preparation and characterization of hexadecyltrimethyl-ammonium bromide modified nanocrystalline cellulose/graphene oxide composite thin film and its potential in sensing copper ion using surface plasmon resonance technique. *Optik* **2018**, *173*, 71–77. [[CrossRef](#)]
57. Zamiranvari, A.; Solati, E.; Dorrani, D. Effect of CTAB concentration on the properties nanosheet produced by laser ablation. *Opt. Laser Technol.* **2017**, *97*, 209–218. [[CrossRef](#)]
58. Rattana, T.; Chaiyakun, S.; Witit-Anun, N.; Nuntawong, N.; Chindaudom, P.; Oaew, S.; Kedkeaw, C.; Limsuwan, P. Preparation and characterization of graphene oxide nanosheets. *Procedia Eng.* **2012**, *32*, 759–764. [[CrossRef](#)]
59. Li, X.; Lao, S.P.; Tang, L.; Ji, R.; Yang, P. Sulphur doping: A facile approach to tune the electronic structure and optical properties of graphene quantum dots. *Nanoscale* **2014**, *6*, 5323–5328. [[CrossRef](#)]
60. Fen, Y.W.; Yunus, W.M.M.; Yusof, N.A.; Ishak, N.S.; Omar, N.A.S.; Zainudin, A.A. Preparation, characterization and optical properties of ionophore doped chitosan biopolymer thin film and its potential application for sensing metal ion. *Optik* **2015**, *126*, 4688–4692. [[CrossRef](#)]

61. Saleviter, S.; Fen, Y.W.; Omar, N.A.; Zainudin, A.A.; Daniyal, W.M.E.M.M. Optical and structural characterization of immobilized 4-(2-pyridylazo) resorcinol in chitosan-graphene oxide composite thin film and its potential for Co^{2+} sensing using surface plasmon resonance technique. *Results Phys.* **2018**, *11*, 118–122. [[CrossRef](#)]
62. Roshidi, M.D.A.; Fen, Y.W.; Omar, N.A.S.; Saleviter, S.; Daniyal, W.M.E.M.M. Optical studies of graphene oxide/poly(amidoamine) dendrimer composite thin film and its potential for sensing Hg^{2+} using surface plasmon resonance spectroscopy. *Sens. Mater.* **2018**, *31*, 1147–1156. [[CrossRef](#)]
63. Hashim, H.S.; Fen, Y.W.; Omar, N.A.S.; Daniyal, W.M.E.M.M.; Saleviter, S.; Abdullah, J. Structural, optical and potential sensing properties of tyrosinase immobilized graphene oxide thin film on gold surface. *Optik* **2020**, *212*, 164786. [[CrossRef](#)]
64. Abdulla, H.S.; Abbo, A.I. Optical and electrical properties of thin films of polyaniline and polypyrrole. *Int. J. Electrochem. Sci.* **2012**, *7*, 10666–10678.
65. Daniyal, W.M.E.M.M.; Fen, Y.W.; Abdullah, J.; Sadrolhosseini, A.R.; Saleviter, S.; Omar, N.A.S. Label-free optical spectroscopy for characterizing binding properties of highly sensitive nanocrystalline cellulose-graphene oxide based nanocomposite towards nickel ion. *Spectrochim. Acta Part A Mol. Biomol. Spectrosc.* **2019**, *212*, 25–31. [[CrossRef](#)]
66. Omar, N.A.S.; Fen, Y.W.; Saleviter, S.; Kamil, Y.M.; Daniyal, W.M.E.M.M.; Abdullah, J.; Mahdi, M.A. Experimental evaluation on surface plasmon resonance sensor performance based on sensitive hyperbranched polymer nanocomposite thin films. *Sens. Actuators A Phys.* **2020**, *303*, 111830. [[CrossRef](#)]
67. Sadrolhosseini, A.; Noor, A.; Bahrami, A.; Lim, H.N.; Talib, Z.A.; Mahdi, M.A. Application of polypyrrole multi-walled carbon nanotube composite layer for detection of mercury, lead and iron ions using surface plasmon resonance technique. *PLoS ONE* **2014**, *9*, e93962. [[CrossRef](#)]



© 2020 by the authors. Licensee MDPI, Basel, Switzerland. This article is an open access article distributed under the terms and conditions of the Creative Commons Attribution (CC BY) license (<http://creativecommons.org/licenses/by/4.0/>).